THE JOURNAL OF PHYSICAL CHEMISTRY C

Article

pubs.acs.org/JPCC

Determination of Nanoparticle Size by Measuring the Metal–Metal Bond Length: The Case of Palladium Hydride

Jianqiang Wang,[†] Qi Wang,[‡] Xinghua Jiang,[†] Zhongneng Liu,[†] Weimin Yang,*[,†] and Anatoly I. Frenkel*[,§]

[†]Sinopec Shanghai Research Institute of Petrochemical Technology, Shanghai 201208, China

[‡]Department of Chemical Engineering, University of Delaware, Newark, Delaware 19717, United States

[§]Physics Department, Yeshiva University, New York, New York 10016, United States

Supporting Information

ABSTRACT: Formation and properties of Pd nanoparticles have been investigated in situ in the temperature range between 186 and 483 K by X-ray absorption fine structure (XAFS) spectroscopy and by ex situ electron microscopy. Results of the experiments conducted under hydrogen and helium atmospheres were compared, in order to illuminate and explain the changes in bond length of Pd particles as a result of hydride formation. By contrasting the data obtained at these two atmospheres we were able to isolate the effects of both the finite particle size and hydrogen absorption on Pd–Pd bond length, obtain hydrogen intake values, and, as a result, estimate the particle size. The calculated average particle size agreed with the electron microscopy data. These results open up new opportunities for in situ size investigations by XAFS of catalytic Pd particles in reaction conditions, when catalyst fragmentation, shape change, and/or coarsening may occur.

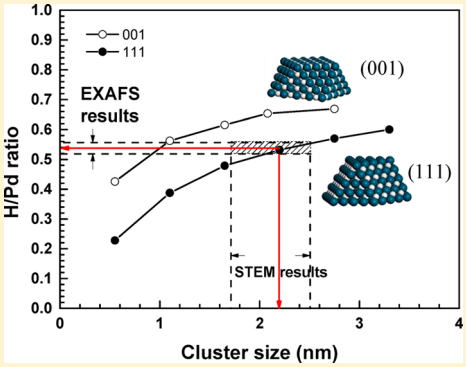

INTRODUCTION

Investigation of size, structure, and electronic properties of catalytic metal nanoparticles is important for understanding mechanisms of catalyst activity, selectivity and deactivation.[1−3] Many advances were achieved in the past decade with the development of synchrotron-based in situ and operando instrumentation that enables multitechnique, correlative studies of catalytic mechanisms.[4−8] Recent developments in instrumentation, data analysis, and modeling methods of extended X-ray absorption fine structure (EXAFS) spectroscopy, one of the premier techniques for catalytic studies, demonstrated its analytical power for measuring the particle size, shape, and structure in the nm-range. Most existing methods of particle size determination by EXAFS rely on the finite size effect that causes the reduction of metal–metal coordination numbers relative to the bulk,[9−12] although alternative approaches have been proposed that rely on the size dependence on other parameters such as, e.g., metal–metal bond length.[13]

These capabilities described above are usually demonstrated in ideal conditions for accurate and unambiguous coordination number measurements (e.g., low temperatures, narrow particle size distributions, and symmetric bond length distributions[14,15]) and are thus not particularly powerful when the catalysts are investigated in reaction conditions that often require high temperature and pressure. An additional complication arises in the case when the particles may undergo size and/or shape change during the reaction, further hindering the accuracy of their characterization.

In this work, we investigate an alternative approach to measure particle size and shape that applies to palladium catalysts in the nanometer size range. Our method is based on the ability of palladium metal to absorb hydrogen and the effect of such absorption on the metal–metal distance. We show that the experimentally measured Pd–Pd bond length can be used as a sensor of hydrogen occupancy that, in turn, can be linked to the particle size via simple structural modeling.

Palladium nanoparticles are widely employed in catalysts for hydro-treatment of petrochemicals,[16,17] synthesis of fine chemicals[18] and purification of automobile exhaust gas,[19] as well as in potential applications for magnetic storage materials[20] and hydrogen storage materials.[21−23] Supported Pd nanocatalysts are among the most frequently used hydrogenation catalysts due to their wide range of processing conditions and superior selectivity.[24−28] While the geometric and electronic structure of pure palladium nanoparticles has been extensively investigated to uncover their effects on catalytic activity,[29−31] relatively little is known to date about the effect of hydrogen absorption on the structure of Pd catalysts in the nm size range.

Since the discovery of hydrogen absorption in bulk palladium in 1866 by Graham,[32] this bulk metal–hydrogen system became a subject of intense research.[33−35] Generally, bulk palladium has the ability to absorb hydrogen to form Pd hydride[36] (α or β-phase) by dissociated hydrogen atoms occupying interstitial sites, which causes metal atoms to be displaced from their ideal sites.[37] A major challenge toward understanding and predicting hydride formation behavior and

Received: October 25, 2014
Revised: December 6, 2014
Published: December 10, 2014

DOI: 10.1021/jp510730a
J. Phys. Chem. C 2015, 119, 854−861

the PdH_x phase diagram in nanocrystalline Pd particles stems from the fact that their thermodynamic properties are different from those of bulk Pd.[38] Bulk palladium has fcc structure with a lattice parameter of 3.890 Å (at 298 K). Upon hydrogen absorption the lattice undergoes an isotropic expansion while retaining its fcc structure[35] with hydrogen atoms occupying some of the octahedral sites.[39] In supported Pd nanoparticles, the Pd lattice structure, modified by interstitial hydrogen, is reported to be similar to the fcc structure of bulk Pd, albeit expanded due to hydrogen absorption.[40] The influence of temperature on the formation and stability of nanoparticles for the metallic state or the hydride state has been reported previously. Yokoyama et al. reported the temperature dependence of Pd K-edge EXAFS of supported Pd catalysts in the metallic state.[41] The formation and stability of Pd hydrides in a well-characterized Pd nanoparticle catalysts have been investigated by using temperatures-programmed reduction and X-ray diffraction.[36] Zizwe et al.[30] measured the lattice expansion at the working conditions at the temperature from ambient to 473 K.

Hydrogen content in Pd hydrides formed from supported Pd catalysts has been shown to be strongly dependent on the particle size.[39,42,43] A dramatic decrease in the hydrogen content of the hydride phases occurs when the Pd crystallite size decreases. In Pd/silica catalyst, the H/Pd ratio in the hydride phase was observed to decrease as a function of Pd dispersion down to 0.55 and thereafter remains constant at 0.3.[44] Pd nanoparticles (5.3 nm in average size), in situ generated inside a mesoporous Zr-modified SiO_2 film, could be transformed into a stable $PdH_{0.70}$ by dipping in aqueous $NaBH_4$ solution.[45] The H/Pd ratio of 0.7 is the largest of all such measurements, regardless of the Pd particle size, in which the H/Pd ratio was studied at room temperature. For example, for Pd foil of 25 μm in thickness, 70% of its octahedral sites were found to be occupied, and the same was obtained for the bulk Pd.[46,47]

In this article, we examined the Pd hydride formation from the well-defined, supported Pd nanoparticles by in situ EXAFS spectroscopy. The H/Pd ratios at temperatures between 186 and 483 K were quantitatively obtained based on the observed lattice expansion. In contrast to other works where bulk Pd lattice parameter is used for computing the H/Pd ratio in nanohydrides, we define lattice expansion with respect to the bare particles of the same size and on the same support, and measured in the same in situ experiment. Due to the surface tension effect that causes reduction of lattice parameter in metal nanoparticles,[13,48] the bare particle of the given size, simulated in our case by using inert gas (helium) environment is a more appropriate reference for the H/Pd ratio measurement than the bulk Pd. Hence, our approach allows to separate the two effects and more accurately obtain the H/Pd ratio from the Pd−Pd bond length.

SAMPLE PREPARATION AND EXPERIMENT

Pd catalysts were prepared by adsorption method from an aqueous solution of $PdCl_2$ in diluted hydrochloric acid on extruded θ-Al_2O_3 support (surface area 90 m^2/g), which yields a Pd weight loading of 0.3%. The supported precursor was dried at 383 K and calcined at 623 K in air. Then the sample was crushed and pressed into a pellet, which was mounted in an in situ XAFS cell (the Nashner-Adler cell).[10] The sample was reduced in situ to form supported Pd nanoparticles by heating in a stream of H_2 (50% in He) to a final temperature of 483 K. XAFS measurements were taken during the reduction process to monitor the degree of reduction.

XAFS measurements were performed at beamlines X18B and X18A at the National Synchrotron Light Source, Brookhaven National Laboratory. A reference Pd foil sample was mounted between the transmission and reference ion chambers. XAFS data in the reference foil were collected simultaneously with the main sample, for energy calibration and alignment. All spectra were collected in transmission mode. The reduction process was monitored by following the changes in the Pd K-edge (at 24,350 eV) region. Thirty min after the white line intensity stabilized at the reduction temperature, full EXAFS scans were taken at a series of temperatures starting at the highest temperature (483 K) and then cooling and stabilizing the Pd absorption peak (also known as "white line") intensity at successively lower temperatures down to 186 K. The data were collected after the temperature was stabilized to within 5 K of the target temperature. After completing the measurements under H_2, the gas flow was switched to ultrahigh purity He. After the end of the series, the temperature was returned to the highest temperature of the series (483 K). EXAFS scans were taken again at 383 K (the temperature was lowered to improve the data quality) to verify the reversibility of the sample. The treatment and measurement cycles are shown schematically in Figure 1.

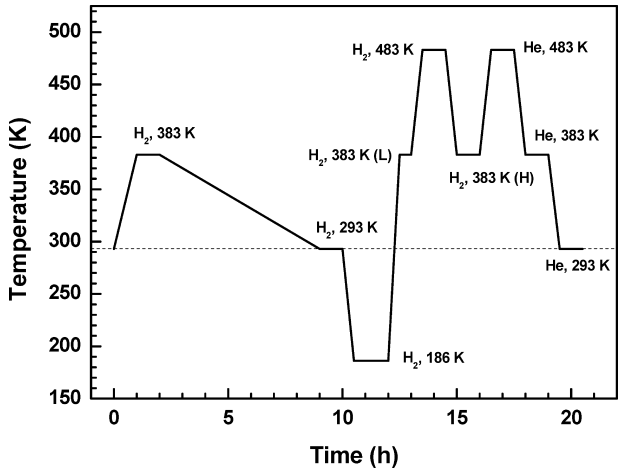

Figure 1. Temperature schedules for in situ gas treatment of Pd catalysts in 50% H_2 in He or pure He at a flow of 50 mL/min and the conditions of all the EXAFS data measured under the atmosphere and the corresponding temperature. L stands for the data repeatedly measured after the lowest temperature of 186 K, and H stands for the one after the highest temperature of 483 K.

X-ray absorption coefficient data were processed and analyzed using the IFEFFIT package.[49−51] All the data were aligned in X-ray energy first. The averaged and background-removed spectra were then normalized using the Athena[49] program. The simultaneous analysis of multiple data sets from different temperatures under the identical atmospheres, were done by fitting theoretical FEFF6 signal to experimental data in R-space, where physically reasonable constraints were applied. The passive electron reduction factor (S_0^2) was set to 0.85 as determined from EXAFS analysis of the Pd foil measured at room temperature in transmission mode. The coordination number (N) and the correction (ΔE) to the threshold energy were varied in the fits but constrained to be the same for all the

DOI: 10.1021/jp510730a
J. Phys. Chem. C 2015, 119, 854−861

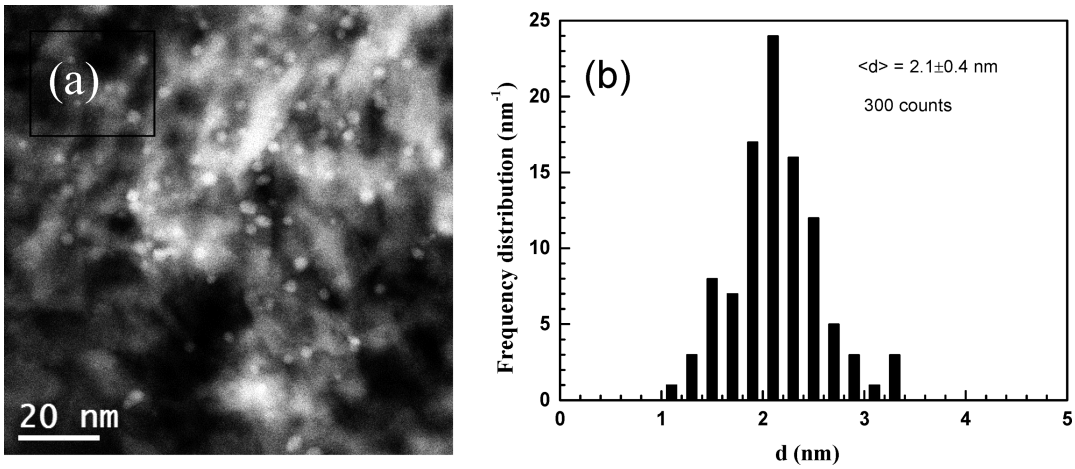

Figure 2. (a) HAADF STEM image of Pd nanoparticles supported on Al_2O_3. The image was taken after reduction in H_2 at 483 K. (b) Histogram of the nanoparticle diameters obtained from STEM images.

data collected at different temperatures. The photoelectron half-path length (R) and the EXAFS Debye–Waller factor (σ^2) were varied individually for different temperatures. A separate fitting model was also used, where a third cumulant of the Pd–Pd nearest neighbor bond distribution was added to other fitting parameters. The best fit results for the third cumulants were found to be consistent with zero, within the error bars, and the model without the third cumulant contribution was chosen as the final fitting model. The k-ranges of the data used in the fit were varied between 2 to 14 and 2 to 15 Å^{-1}, depending on the conditions.

The samples after the treatment were examined by electron microscopy. A drop of the suspension of powder in acetone was deposited on copper grids coated with an ultrathin carbon film on holey carbon. Dark-field images were obtained by using a JEOL 2200MCO (S) TEM (Brookhaven National Laboratory) which is operated at 200 kV. The images were analyzed using Digital Micrograph (Gatan, Inc.), and the diameters of individual particles were determined using intensity profiles. The error associated with measurement of the average nanocluster size was taken as one standard deviation (Figure 2).

RESULTS

Dark-field STEM micrograph of Pd nanoparticles on θ-Al_2O_3 support obtained after the EXAFS measurement is shown in Figure 2a. Reduction of the supported PdO at 483 K, at a loading of 0.3 wt % Pd, resulted in well-dispersed nanoparticles (Figure 2a). A narrow distribution of particle sizes in the range of 1.1–3.4 nm was observed (Figure 2b) and the mean particle diameter was determined to be 2.1 ± 0.4 nm, by counting about 300 Pd nanoparticles. No aggregation was detected. The data reversibility of EXAFS analysis at high temperature (483 K) before and after H_2/He treatment verified the stability of such nanoparticles (SI, Figure S1).

X-ray absorption near-edge structure (XANES) data demonstrate that a complete disappearance of the Pd oxide phase and the formation of the reduced Pd state were observed as the system was subjected to reduction by 50% H_2/He at 483 K (SI, Figure S2). The stability (lack of growth) of Pd hydride nanoparticles was confirmed by examining several XANES and EXAFS data sets measured at the same temperature (383 K) before and after the cooling and heating cycles in H_2 (SI, Figure S1 and Figure S2).

Both the raw EXAFS data $\chi(k)$ and its Fourier transform amplitude provide useful insights into the influences of temperature and hydrogen effects on structural and dynamic properties of the nanoparticles. Figure 3a presents progressive changes in intensity of the EXAFS data in k-space on the Pd/Al_2O_3 sample in response to the temperature variation in helium. Reductions in oscillation intensity, especially pronounced in high k-range, and in the FT magnitudes, observed

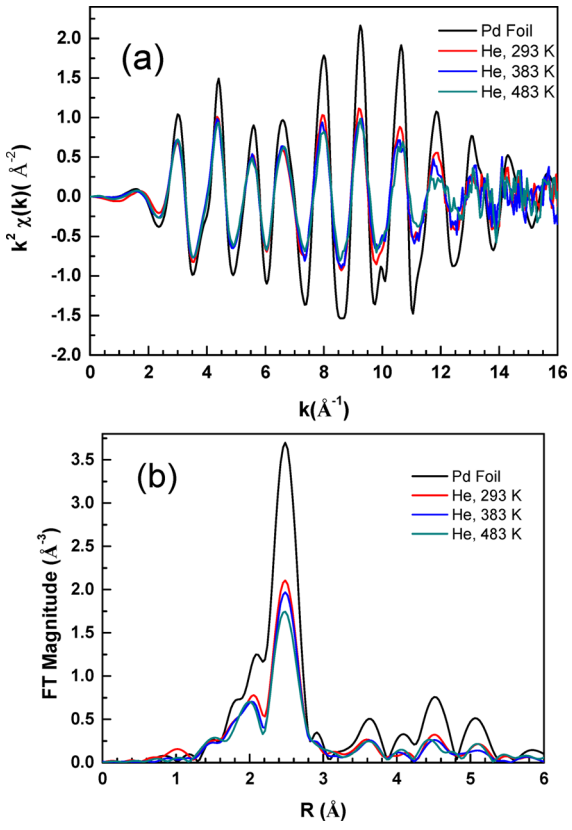

Figure 3. (a) Progressive changes in intensity of the EXAFS data in k-space on the Pd/Al_2O_3 sample (k-weight = 2 and k-range = 2–16 Å^{-1}) in response to temperature variation in helium and (b) corresponding Fourier transform magnitudes with gradual changes in real space. The bulk Pd foil spectra measured at room temperature are included for comparison.

DOI: 10.1021/jp510730a
J. Phys. Chem. C 2015, 119, 854–861

at elevated temperatures are consistent with the temperature-induced increase of the bond length disorder. As evidenced from the peak position in corresponding R-space data (Figure 3b), there is no apparent change in the bond length during the helium cycle.

EXAFS data obtained in hydrogen cycle are shown in Figure 4. At lower temperatures, the oscillation frequency is distinctly

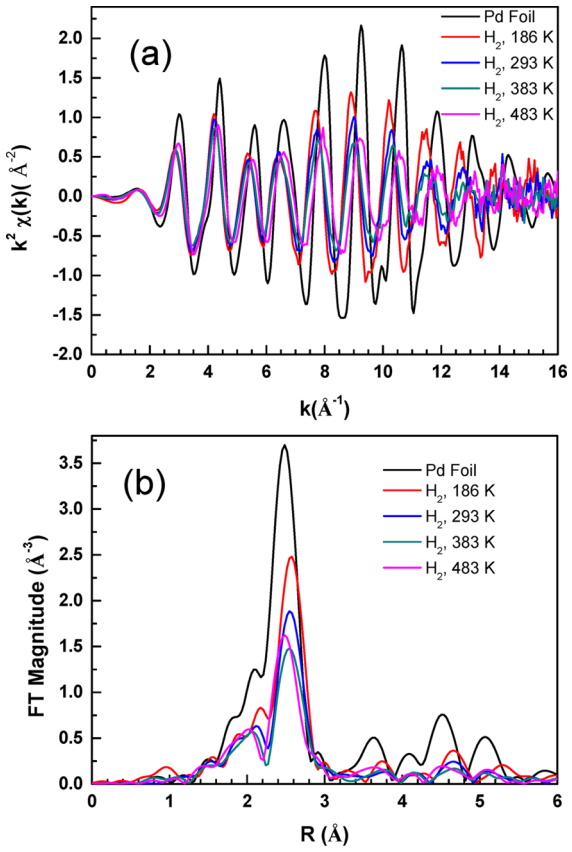

Figure 4. (a) EXAFS data in *k*-space illustrating the effect of temperature on the oscillatory pattern of Pd nanoparticles and a bulk foil standard (*k*-weight = 2 and *k*-range = 2−16 $Å^{-1}$) with corresponding (b) Fourier transform magnitudes.

higher (and the bond length, correspondingly, longer), as reflected in the *k*-space (Figure 4a) and *r*-space (Figure 4b) behavior, respectively. As the temperature increases, the oscillatory pattern in *k*-space shifts closer to that in Pd foil, measured at room temperature, and the oscillation intensity decreases with temperature gradually, as expected for thermal disorder effect, except that the EXAFS data at 483 K shows a sudden increase in intensity and a marked drop in Pd−Pd distance (Figure 4b). This behavior is consistent with gradual desorption of hydrogen with temperature, with the most rapid change in hydrogen concentration occurring between 383 and 483 K. SI Figure S3 demonstrates that the data for the two states of the sample, in H_2 and in He, at 483 K agree well in energy, *k*- and *r*-spaces. Hence, we conclude that the H/Pd ratio should be very low in the sample under H_2 atmosphere at that temperature.

The quantitative results of the data analyses for all the EXAFS data both in hydrogen and helium are summarized in Table 1, and the Pd−Pd bond lengths are plotted in Figure 5. The values of the average first-nearest-neighbor (1NN) Pd−Pd coordination numbers (~9.3) demonstrate surface truncation

Table 1. EXAFS Analysis Results: the First Nearest Neighbor Coordination Number, Distance, Its Mean Squared Disorder, the Total and Reduced Chi Squared, and the R-Factor[a]

regime	CN	*R* (Å)	σ^2 ($Å^2$)	χ^2	χ_ν^2	*R*-factor
H_2, 483 K	9.3(2)	2.748(2)	0.0096(2)	997.7	12.9	0.009
H_2, 383 K		2.799(3)	0.0093(3)			
H_2, 293 K		2.813(2)	0.0080(2)			
H_2, 186 K		2.826(1)	0.0061(2)			
He, 483 K	9.2(2)	2.733(2)	0.0089(2)	811.8	16.3	0.008
He, 383 K		2.741(2)	0.0081(2)			
He, 293 K		2.741(1)	0.0075(2)			

[a]The chi squared and R-factor values refer to the entire series of data analyzed concurrently (either in hydrogen or in helium). Coordination numbers were constrained to be the same for the entire series, as described in the text. Uncertainties in the last significant digits are shown in parentheses.

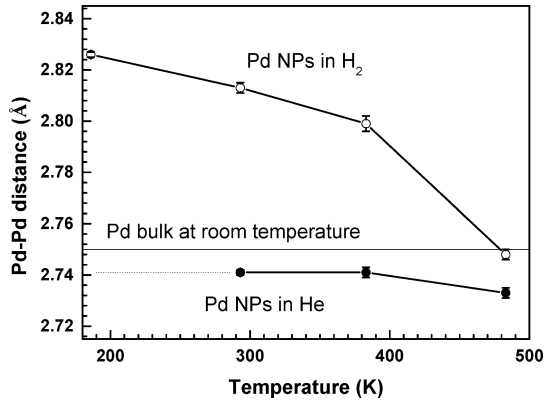

Figure 5. Pd−Pd bond lengths at different temperatures and atmospheres (H_2 and He). Extrapolation to the low temperatures is shown by dotted line for He atmosphere.

effect that enables further analysis of the coordination numbers in terms of the representative nanoparticle sizes. These numerical results from quantitative analysis confirm preliminary conclusions based on visual observation of the data. Namely, the results show several distinct effects:

A contraction of nanoparticle bond lengths compared to the bulk. The Pd−Pd bond length was obtained to be 2.741 ± 0.001 Å for nanoparticles measured in He at ambient conditions, which is smaller than the 2.750 Å value characterizing bulk Pd measured at the same temperature.

A decrease of the Pd−Pd distance in He atmosphere as the temperature is increased from 293 to 483 K (Figure 5). A similar behavior ("a negative thermal bond length expansion"), which was attributed to the enhanced mobility of particles on the support at elevated temperatures and strongly nonvibrational dynamics[52,53] was observed previously for alumina-supported Pt nanoparticles in He atmosphere.

A more significant decrease of the Pd−Pd distance from 186 to 483 K (Figure 5) was observed in H_2 environment. This decrease of the bond length corroborates the visible trends in the *r*-space. Notably, XAFS features in *R*-space become progressively more similar to those in He as the temperature increases. Such behavior is attributed to the temperature-induced desorption of hydrogen, which causes the shortening of the Pd−Pd bond length as the H/Pd ratio decreases.

DOI: 10.1021/jp510730a
J. Phys. Chem. C 2015, 119, 854−861

We note that the data (Table 1 and Figure 5) demonstrate that the H/Pd ratio at 483 K is greater than zero. The reason for that is the non-negligible difference between the Pd−Pd distances in H_2 and He at that temperature. Specifically, the best fit value of the Pd−Pd length under H_2 (2.748 ± 0.002 Å) was obtained to be 0.015 Å larger than that under He (2.733 Å ± 0.002). The discrepancy indicates that some amount of hydrogen was still present in the sample at that temperature and is factored in when estimating uncertainties in the H/Pd ratio reported in this work.

DISCUSSION

1. Evaluation of the H/Pd Ratio at Different Temperatures. The expansion of the lattice (δR) in Pd hydride is linked to the H/Pd ratio by the following empirical equation:[30,54]

$$\frac{\delta R(T)}{R(T)} = 0.0666x - 0.0164x^2 \quad (1)$$

where x is the H/Pd ratio and R is the bond length of bare metal particles free of hydrogen. Equation 1 has been used frequently in studies of H/Pd ratio in Pd hydrides of different dimensionality.[30] While δR can be measured accurately by EXAFS at different temperatures, the effects of factors other than H absorption on Pd−Pd bond length change with temperature have not been systematically investigated. Among such factors are the lattice contraction, a universal effect of small (under 5 nm in size) metal nanoparticles due to their large surface tension,[48] as well as the interaction with support and adsorbate that may affect the bond length as well.[53,55,56] These effects are very complex and may have a complicated temperature dependence that is not known a priori. Together, these difficulties in determining both δR and R as a function of temperature make the determination of H/Pd ratio in nanoparticles with eq 1 ambiguous. A reliable measurement of δR and, hence, x at all temperatures will be guaranteed only when the Pd−Pd bond length in hydrogen absorption conditions is compared with that in the absence of hydrogen, in otherwise equivalent conditions (the same particle size distribution, support material, and temperature). In the present work this condition is met by contrasting the data collected in H_2 and inert (He) atmosphere at the same temperatures. Due to the clear evidence of nonbulk effects in He atmosphere (Figure 5), our method thus provides the needed accuracy because we compare the expanded bond length (under hydrogen) to its reference value for the same particle size. Clearly, it shows the amount of hydrogen absorbed into Pd nanoparticles. We used the bond lengths at different temperatures and atmospheres to calculate the ratios of H/Pd (SI, Table S1 and Figure 6).

2. Determination of the Cluster Size from the H/Pd Ratio in nm-Size Metal Particles. The number of interior octahedral sites available for hydrogen incorporation in Pd hydrides and, hence, the H/Pd ratio, is expected to decrease gradually as the particle size decreases (due to the decrease of the volume to surface ratio at small particles). That universal property can be used to estimate the particle size from the measured value of the H/Pd ratio, provided that the relevant experimental data describing a "representative" particle of a certain size exists. EXAFS is an ensemble-average technique and the Pd−Pd bond lengths and the coordination numbers are obtained over all Pd-containing species in the sample. However, when the particle size distributions are narrow, EXAFS results can be used for quantitative determination of particle sizes and shapes[9,10] in controlled atmospheres and even in reaction conditions.[57,58] Due to the narrow particle size distribution (Figure 2b), we are able to compare computer-generated cluster models, and the numerical results on the H/Pd ratio and Pd−Pd coordination numbers with the average size of the "representative nanoparticles" obtained by STEM.

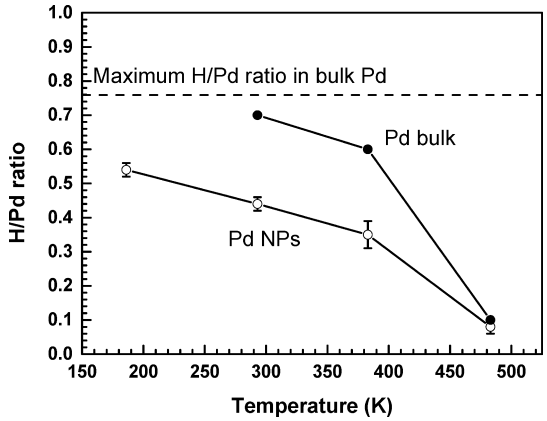

Figure 6. Ratio of H/Pd for 2.1 nm nanoparticles and bulk Pd inferred from ref 47 as a function of temperature.

The modeling of the clusters of different sizes and morphologies was done using Materials Studio software. The number of H atoms in each cluster model was calculated assuming full occupancy on interior octahedral sites and then multiplied by 0.76 for calculating the maximum possible H/Pd ratio in nanoclusters, as described in greater detail below.

Several models of truncated hemispherical cuboctahedra possessing fcc structure and belonging to two series, one with support surface having (001), and the other (111) orientation, were constructed using the EXAFS derived Pd−Pd bond lengths under hydrogen (at 186 K). Only one model from each series agreed, within the error bars, with both the EXAFS-determined coordination number of Pd−Pd pairs, 9.2, and STEM results for the average particle diameter of 2.1 nm. The structural parameters derived from these two models are compared with the experimental results, which are listed in Table 2.

Table 2. Theoretical Models and Their Comparisons with XAFS and STEM Data

Properties	[a]Data.	[b]Model			
	He, 293 K	(001)		(111)	
Clusters	-				
Size (nm)	2.1	2.8	2.2	2.8	2.2
CN	9.2(2)	9.38	8.87	9.39	8.89
Atoms	-	311	175	326	185

[a]Nanoparticle size was measured by STEM; coordination number (CN) of the first nearest neighbors was obtained for the EXAFS data measured under He at 293 K.. [b]Cluster models of different sizes (between 2.2 and 2.8 nm), surface morphologies and support orientations ((111) or (001) oriented) were constructed by Materials Studio software.

DOI: 10.1021/jp510730a
J. Phys. Chem. C 2015, 119, 854−861

The upper limit of hydrogen absorption in Pd at ambient temperature and pressure corresponds to the $PdH_{0.70}$ material, indicating that approximately 70% of the octahedral holes are occupied.[47,59] To the best of our knowledge, there are no reports on PdH_x isotherms at temperatures lower than room temperature. However, a relatively large H/Pd ratio could be obtained by Pd hydrogenation at 4 MPa and 573 K or even higher.[60,61] In those experiments,[60,61] after the hydrogen concentration was obtained to be 0.764 at ambient temperature and pressure, after the high temperature and high pressure treatments. It is also known that PdH_x could be stored in liquid nitrogen (77 K) without the loss of hydrogen[60] and is also stable over the temperature range between 4 and 300 K.[61] Figure 6 demonstrates that the experimental H/Pd curve in Pd nanoparticles reaches a much lower value (ca. 0.54) than the bulk's 0.76 hydrogen occupancy limit at 186 K. We note that that experimental ratio was obtained using extrapolated, not actual, value of Pd−Pd bonds under He atmosphere at 186 K. That is a reasonable approximation because the actual values should be very close to each other, within the experimental uncertainties, based on the trend shown in Figure 5. In the models of nanoclusters used for the particle size determination (vide infra) we will use the 0.76 value as the maximum occupancy because our models will correspond to the lowest temperatures in which the H/Pd ratios can be measured most accurately. We note here that our results will not change significantly (within a 10% relative error, at the most) if we used the actual, not extrapolated, bond length values (e.g., at room temperatures), and the corresponding maximum bulk H occupancy of 0.7, not 0.76.

The observation (Figure 6) that the H/Pd ratio is much smaller, at the same temperatures, in the nanoparticles, compared to the bulk Pd, is related to the finite size effects in the nanopartilces, where surface Pd atoms have fewer H neighbors than the interior Pd atoms.

The values for the H/Pd ratios were calculated for each cluster model and plotted in Figure 7. Calculations demonstrate that the estimated x will be 0.52 for the (111)-oriented clusters, and 0.65 for the (001)-oriented clusters of ca. 2.1 nm in size. The latter value of x is far beyond the experimental value of 0.54 ± 0.02 at 186 K (Table 2). Hence, the (111)-oriented clusters are a better match to the experimental data. As a result, the particle size of 2.1 ± 0.4 nm obtained by STEM is in agreement with the particle size that is inferred from the experimentally determined H/Pd ratio of 0.54 ± 0.02. Hence, the experimental H/Pd ratio determined by expansion of bond length can be used to estimate the particle size by occupancy model calculation. It should be noted that only for particle sizes below 3 nm this method is effective because x varies strongly with size in this size range.

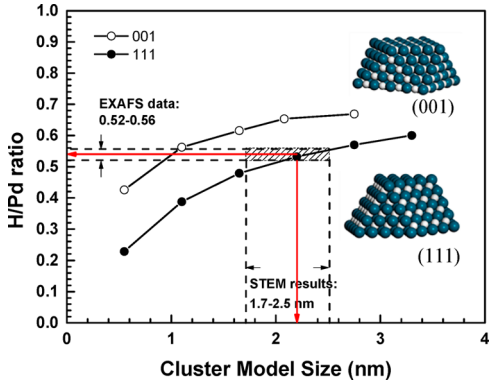

Figure 7. Determination of the model cluster sizes (shown for two different types) using the H/Pd ratio obtained from the measured Pd−Pd distances. The 111 model fits the data (shown by red arrows) for both the H/Pd ratio at 186 K and the particle size range, while the 001 model does not.

This method of particle size estimation by in situ EXAFS analysis, through the Pd−Pd bond length measurement in nanoscale Pd hydrides at different temperatures, offers a potentially useful alternative to other techniques used for particle size determination. One possible application could be its use in the in situ or operando catalysis studies, in which the particle size may change in the course of the reaction. In order to evaluate the average Pd particle size by EXAFS, the hydrogen−helium substitution scheme described in this work can be used at each stage of the reaction. First, the sample would be heated to reduce Pd catalysts, and then cooled in hydrogen atmosphere, followed by another heating cycle in which hydrogen will be replaced by He at high temperature, and the sample will be cooled again, this time in He. In the both cases, the EXAFS data obtained at the lowest temperature (e.g., a cryogenic, or room temperature, depending on the experimental conditions and reactors used) under H_2 and He will be analyzed the same way shown in our work, to obtain the H/Pd ratio and, from it, the average particle size.

CONCLUSIONS

The Pd−Pd bond lengths of the 2.1 ± 0.4 nm Pd nanoparticles were measured by X-ray absorption spectroscopy at different temperatures and atmospheres (hydrogen and helium). Based on the observed expansion of the Pd−Pd bond length at lower temperatures, a ratio of H/Pd was calculated for each temperature and compared with several cluster models of different sizes and shapes. Truncated hemispherical cuboctahedral particle model, with (111) surface orientation, was the best match to the experimentally obtained H/Pd ratio and the STEM-measured particle size distribution. The present method could be extended to in situ studies of supported Pd particles in different stages of catalytic reactions.

ASSOCIATED CONTENT

Supporting Information

Graphs of the raw data of X-ray absorption coefficients, the background-subtracted, edge-step normalized EXAFS data in k-space and r-space, and the calculations of the H/Pd ratio at different temperatures. This material is available free of charge via the Internet at http://pubs.acs.org.

AUTHOR INFORMATION

Corresponding Authors

*E-mail: yangwm.sshy@sinopec.com.
*E-mail: anatoly.frenkel@yu.edu.

Notes

The authors declare no competing financial interest.

ACKNOWLEDGMENTS

This work was supported in part by Sinopec SRIPT. A.I.F. acknowledges support from the Chemical Sciences, Geosciences, and Biosciences Division, Office of Basic Energy Sciences, Office of Science, U.S. Department of Energy, Grant No. DE-FG02-03ER15476. Use of the NSLS is supported by

DOI: 10.1021/jp510730a
J. Phys. Chem. C 2015, 119, 854−861

the U.S. Department of Energy, Office of Science, Office of Basic Energy Sciences, under Contract No. DE-AC02-98CH10886. Beamline X18B at the NSLS is supported in part by the Synchrotron Catalysis Consortium, U.S. Department of Energy Grant No. DE-FG02-05ER15688. The authors are grateful to Dr. C. Ma for the analysis of electron microscopy images and Dr. X. J. Wang for assistance in sample preparation and in situ EXAFS measurements.

REFERENCES

(1) Cargnello, M.; Doan-Nguyen, V. V. T.; Gordon, T. R.; Diaz, R. E.; Stach, E. A.; Gorte, R. J.; Fornasiero, P.; Murray, C. B. Control of Metal Nanocrystal Size Reveals Metal-Support Interface Role for Ceria Catalysts. *Science* **2013**, *341*, 771−773.

(2) Astruc, D. *Nanoparticles and catalysis*; Wiley-VCH: Weinheim, Germany, 2008.

(3) Bell, A. T. The Impact of Nanoscience on Heterogeneous Catalysis. *Science* **2003**, *299*, 1688−1691.

(4) Wang, X.; Hanson, J. C.; Frenkel, A. I.; Kim, J.-Y.; Rodriguez, J. A. Time-resolved Studies for the Mechanism of Reduction of Copper Oxides with Carbon Monoxide: Complex Behavior of Lattice Oxygen and the Formation of Suboxides. *J. Phys. Chem. B* **2004**, *108*, 13667−13673.

(5) Yano, J.; Yachandra, V. K.; Kanan, M. W.; Surendranath, Y.; Dinca, M.; Nocera, D. G. "An Artificial Water-Oxidizing Co Electro-Catalyst: Structure and Mechanism by *in situ* X-ray Absorption Spectroscopy." *Photosynthesis Research for Food, Fuel and the Future*. Springer: Berlin, 2013; pp 266−268.

(6) Nagai, Y.; Dohmae, K.; Nishimura, Y. F.; Kato, H.; Hirata, H.; Takahashi, N. Operando XAFS Study of Catalytic NO Reduction over Cu/CeO_2: the Effect of Copper−Ceria Interaction under Periodic Operation. *Phys. Chem. Chem. Phys.* **2013**, *15*, 8461−8465.

(7) Patlolla, A.; Baumann, P.; Xu, W.; Senanayake, S. D.; Rodriguez, J. A.; Frenkel, A. I. Characterization of Metal-Oxide Catalysts in Operando Conditions by Combining X-ray Absorption and Raman Spectroscopies in the Same Experiment. *Top. Catal.* **2013**, *56*, 896−904.

(8) Parlett, C.; Gaskell, C. V.; Naughton, J. N.; Newton, M. A.; Wilson, K.; Lee, A. F. Operando Synchronous DRIFTS/MS/XAS as a Powerful Tool for Guiding the Design of Pd Catalysts for the Selective Oxidation of Alcohols. *Catal. Today* **2013**, *205*, 76−85.

(9) Frenkel, A. I. Solving the Structure of Nanoparticles by Multiple-Scattering EXAFS Analysis. *J. Synchrotron Radiat.* **1999**, *6*, 293−295.

(10) Frenkel, A. I.; Hills, C. W.; Nuzzo, R. G. A View from the Inside: Complexity in the Atomic Scale Ordering of Supported Metal Nanoparticles. *J. Phys. Chem. B* **2001**, *105*, 12689−12703.

(11) Calvin, S.; Miller, M. M.; Goswami, R.; Cheng, S. F.; Mulvaney, S. P.; Whitman, L. J.; Harris, V. G. Determination of Crystallite Size in a Magnetic Nanocomposite Using Extended X-ray Absorption Fine Structure. *J. Appl. Phys.* **2003**, *94*, 778−783.

(12) Jentys, A. Estimation of Mean Size and Shape of Small Metal Particles by EXAFS. *Phys. Chem. Chem. Phys.* **1999**, *1*, 4059−4063.

(13) Frenkel, A. I.; Nemzer, S.; Pister, I.; Soussan, L.; Harris, T.; Sun, Y.; Rafailovich, M. H. Size-Controlled Synthesis and Characterization of Thiol-Stabilized Gold Nanoparticles. *J. Chem. Phys.* **2005**, *123*, 184701−1−184701−6.

(14) Yevick, A.; Frenkel, A. I. Effects of Surface Disorder on EXAFS Modeling of Metallic Clusters. *Phys. Rev. B* **2010**, *81*, 115451−1−115451−7.

(15) Yancey, D. F.; Chill, S. T.; Zhang, L.; Frenkel, A. I.; Henkelman, G.; Crooks, R. M. A Theoretical and Experimental Examination of Systematic Ligand-Induced Disorder in Au Dendrimer-Encapsulated Nanoparticles. *Chem. Sci.* **2013**, *4*, 2912−2921.

(16) Teschner, D.; Borsodi, J.; Wootsch, A.; Révay, Z.; Hävecker, M.; Knop-Gericke, A.; Jackson, S. D.; Schlögl, R. The Roles of Subsurface Carbon and Hydrogen in Palladium-Catalyzed Alkyne Hydrogenation. *Science* **2008**, *320*, 86−89.

(17) Okada, T.; Kim, Y.; Sainoo, Y.; Komeda, T.; Trenary, M.; Kawai, M. Coexistence and Interconversion of Di-σ and π-Bonded Ethylene on the Pt(111) and Pd(110) Surfaces. *J. Phys. Chem. Lett.* **2011**, *2*, 2263−2266.

(18) Pellegrini, R.; Agostini, G.; Groppo, E.; Piovano, A.; Leofanti, G.; Lamberti, C. 0.5 wt.% Pd/C Catalyst for Purification of Terephthalic Acid: Irreversible Deactivation in Industrial Plants. *J. Catal.* **2011**, *280*, 150−160.

(19) Nishihata, Y.; Mizuki, J.; Akao, T.; Tanaka, H.; Uenishi, M.; Kimura, M.; Okamoto, T.; Hamada, N. Self-Regeneration of a Pd-Perovskite Catalyst for Automotive Emissions Control. *Nature* **2002**, *418*, 164−167.

(20) Taniyama, T.; Ohta, E.; Sato, T. Observation of 4d Ferromagnetism in Free-Standing Pd Fine Particles. *Eruophys. Lett.* **1997**, *38*, 195−200.

(21) Sun, Y.; et al. Characterization of Palladium Nanoparticles by Using X-ray Reflectivity, EXAFS, and Electron Microscopy. *Langmuir* **2006**, *22*, 807−816.

(22) Király, Z.; Mastalir, Á.; Berger, F.; Dékány, I. Sorption and Microcalorimetric Investigations of Palladium/Hydrogen Interactions on Palladium−Graphimet Intercalation Catalyst. *Langmuir* **1997**, *13*, 465−468.

(23) Király, Z.; Mastalir, Á.; Berger, F.; Dékány, I. Calorimetric Study of Sorption of Hydrogen by Carbon-Supported Palladium. *Langmuir* **1998**, *14*, 1281−1282.

(24) Teixeira, L. S.; Souza, J. C.; dos Santos, H. C.; Pontes, L. A.; Guimarães, P. R.; Sobrinho, E. V.; Vianna, R. F. The Influence of Cu, Fe, Ni, Pb and Zn on Gum Formation in the Brazilian Automotive Gasoline. *Fuel Process. Technol.* **2007**, *88*, 73−76.

(25) Dryer, C.; Lowry, C.; Morrell, J. C.; Egloff, G. Mechanism of Gum Formation in Cracked Gasoline-Formation of Peroxide, Aldehyde, and Acid in Storage. *Ind. Eng. Chem.* **1934**, *26*, 885−888.

(26) Tukač, V.; Handlová, M.; Chyba, V.; Lederer, J.; Kolena, J.; Kubička, D.; Hanika, J.; Jiřičný, V.; Stavárek, P. *Eur. Cong. Chem. Eng. (ECCE-6) Copenhagen* **2007**, 16−20.

(27) Walters, E.; Minor, H.; Yabroff, D. Chemistry of Gum Formation in Cracked Gasoline. *Ind. Eng. Chem.* **1949**, *41*, 1723−1729.

(28) Pereira, R. C.; Pasa, V. Effect of Mono-Olefins and Diolefins on the Stability of Automotive Gasoline. *Fuel* **2006**, *85*, 1860−1865.

(29) Srabionyan, V. V.; Bugaev, A. L.; Pryadchenko, V. V.; Avakyan, L. A.; van Bokhoven, J. A.; Bugaev, L. A. EXAFS Study of Size Dependence of Atomic Structure in Palladium Nanoparticles. *J. Phys. Chem. Solids* **2014**, *75*, 470−476.

(30) Chase, Z. A.; Fulton, J. L.; Camaioni, D. M.; Mei, D.; Balasubramanian, M.; Pham, V.-T.; Zhao, C.; Weber, R. S.; Wang, Y.; Lercher, J. A. State of Supported Pd During Catalysis in Water. *J. Phys. Chem. C* **2013**, *117*, 17603−17612.

(31) Wilde, M.; Fukutani, K.; Naschitzki, M.; Freund, H. J. Hydrogen Absorption in Oxide-Supported Palladium Nanocrystals. *Phys. Rev. B* **2008**, *77*, 113412−1−113412−4.

(32) Graham, T. On the Absorption and Dialytic Separation of Gases by Colloid Septa. *Philos. Trans. R. Soc. London* **1866**, *156*, 399−439.

(33) Lewis, F. A. The Hydrides of Palladium and Palladium Alloys. *Platinum Metals Rev.* **1961**, *5*, 21−25.

(34) Lewis, F. A. The Palladium-Hydrogen System. *Platinum Metals Rev.* **1982**, *26*, 20−27.

(35) Flanagan, T. B.; Oates, W. A. The Palladium-Hydrogen System. *Annu. Rev. Mater. Sci.* **1991**, *21*, 269−304.

(36) Nag, N. K. A Study on the Formation of Palladium Hydride in a Carbon-Supported Palladium Catalyst. *J. Phys. Chem. B* **2001**, *105*, 5945−5949.

(37) Suleiman, M.; Jisrawi, N. M.; Dankert, O.; Reetz, M. T.; Bähtz, C.; Kirchheim, R.; Pundt, A. Phase Transition and Lattice Expansion During Hydrogen Loading of Nanometer Sized Palladium Clusters. *J. Alloys Compd.* **2003**, *644*, 356−357.

(38) McCaulley, J. A. Temperature Dependence of the Pd K-Edge Extended X-ray Absorption Fine Structure of PdC_x (x~0.13). *Phys. Rev. B* **1993**, *47*, 4873−4879.

DOI: 10.1021/jp510730a
J. Phys. Chem. C 2015, 119, 854−861

(39) Tew, M. W.; Miller, J. T.; van Bokhoven, J. A. Particle Size Effect of Hydride Formation and Surface Hydrogen Adsorption of Nanosized Palladium Catalysts: L3 Edge vs K Edge X-ray Absorption Spectroscopy. *J. Phys. Chem. C* **2009**, *113*, 15140−15147.
(40) Davis, R. J.; Landry, S. M.; Horsley, J. A.; Boudart, M. X-ray Absorption Study of the Interaction of Hydrogen with Clusters of Supported Palladium. *Phys. Rev. B* **1989**, *39*, 10580−10583.
(41) Yokoyama, T.; Kimoto, S.; Ohta, T. Temperature-Dependent EXAFS Study on Supported Silver and Palladium Clusters. *Jpn. J. Appl. Phys.* **1989**, *28*, L851−L853.
(42) Morkel, M.; Rupprechter, G.; Freund, H.-J. Finite Size Effects on Supported Pd Nanoparticles: Interaction of Hydrogen with CO and C_2H_4. *Surf. Sci.* **2005**, *588*, L209−L219.
(43) Rupprechter, G. A Surface Science Approach to Ambient Pressure Catalytic Reactions. *Catal. Today* **2007**, *126*, 3−17.
(44) Sepúlveda, J. H.; Fígoli, N. S. The Influence of Calcination Temperature on Pd Dispersion and Hydrogen Solubility in Pd/SiO_2. *Appl. Surf. Sci.* **1993**, *68*, 257−264.
(45) Saha, J.; Dandapat, A.; De, G. Transformation of Pd → $PdH_{0.7}$ Nanoparticles Inside Mesoporous Zr-Modified SiO_2 Films in Ambient Conditions. *J. Mater. Chem.* **2011**, *21*, 11482−11485.
(46) Seymour, E. F. W.; Cotts, R. M.; Williams, W. D. NMR Measurement of Hydrogen Diffusion in β-Palladium Hydride. *Phys. Rev. Lett.* **1975**, *35*, 165−167.
(47) Frieske, H.; Wicke, E. Magnetic Susceptibility and Equilibrium Diagram of PdH_n. *Ber. Bunsen-Ges. Phys. Chem.* **1973**, *77*, 48−52.
(48) Mays, C. W.; Vermaak, J. S.; Kuhlmann-Wilsdorf, D. On Surface Stress and Surface Tension: II. Determination of the Surface Stress of Gold. *Surf. Sci.* **1968**, *12*, 134−140.
(49) Newville, M. IFEFFIT: Interactive XAFS Analysis and FEFF Fitting. *J. Synchrotron Radiat.* **2001**, *8*, 322−324.
(50) Ravel, B.; Newville, M. ATHENA, ARTEMIS, HEPHAESTUS: Data Analysis for X-ray Absorption Spectroscopy Using IFEFFIT. *J. Synchrotron Radiat.* **2005**, *12*, 537−541.
(51) Newville, M.; Livins, P.; Yacoby, Y.; Rehr, J. J.; Stern, E. A. Near-Edge X-ray-Absorption Fine Structure of Pb: A Comparison of Theory and Experiment. *Phys. Rev. B* **1993**, *47*, 14126−14131.
(52) Kang, J. H.; Menard, L. D.; Nuzzo, R. G.; Frenkel, A. I. Unusual Non-Bulk Properties in Nanoscale Materials: Thermal Metal-Metal Bond Contraction of γ-Alumina-Supported Pt Catalysts. *J. Am. Chem. Soc.* **2006**, *128*, 12068−12069.
(53) Sanchez, S. I.; Menard, L. D.; Bram, A.; Kang, J. H.; Small, M. W.; Nuzzo, R. G.; Frenkel, A. I. The Emergence of Nonbulk Properties in Supported Metal Clusters: Negative Thermal Expansion and Atomic Disorder in Pt Nanoclusters Supported on γ-Al_2O_3. *J. Am. Chem. Soc.* **2009**, *131*, 7040−7054.
(54) Feenstra, R.; Griessen, R.; De Groot, D. G. Hydrogen Induced Lattice Expansion and Effective HH Interaction in Single Phase PdH_c. *J. Phys. F: Met. Phys.* **1986**, *16*, 1933−1952.
(55) Small, M. W.; Sanchez, S. I.; Marinkovic, N. S.; Frenkel, A. I.; Nuzzo, R. G. Influence of Adsorbates on the Electronic Structure, Bond Strain, and Thermal Properties of an Alumina-Supported Pt Catalyst. *ACS Nano* **2012**, *6*, 5583−5595.
(56) Nosova, L. V.; Stenin, M. V.; Nogin, Y. N.; Ryndin, Y. A. EXAFS and XPS Studies of the Influence of Metal Particle Size, Nature of Support and H_2 and CO Adsorption on the Structure and Electronic Properties of Palladium. *Appl. Surf. Sci.* **1992**, *55*, 43−48.
(57) Roldan Cuenya, B.; Croy, J. R.; Mostafa, S.; Behafarid, F.; Li, L.; Zhang, Z.; Yang, J. C.; Wang, Q.; Frenkel, A. I. Solving the Structure of Size-Selected Pt Nanocatalysts Synthesized by Inverse Micelle Encapsulation. *J. Am. Chem. Soc.* **2010**, *132*, 8747−8756.
(58) Mostafa, S.; Behafarid, F.; Croy, J. R.; Ono, L. K.; Li, L.; Yang, J. C.; Frenkel, A. I.; Cuenya, B. R. Shape-Dependent Catalytic Properties of Pt Nanoparticles. *J. Am. Chem. Soc.* **2010**, *132*, 15714−15719.
(59) Worsham, J. E., Jr; Wilkinson, M. K.; Shull, C. G. Neutron-Diffraction Observations on the Palladium-Hydrogen and Palladium-Deuterium Systems. *J. Phys. Chem. Solids* **1957**, *3*, 303−310.
(60) Ross, D. K.; Antonov, V. E.; Bokhenkov, E. L.; Kolesnikov, A. I.; Ponyatovsky, E. G.; Tomkinson, J. Strong Anisotropy in the Inelastic Neutron Scattering from PdH at High Energy Transfer. *Phys. Rev. B* **1998**, *58*, 2591−2595.
(61) Nygren, L. A.; Leisure, R. G. Elastic Constants of α'-phase PdH_x over the Temperature Range 4−300 K. *Phys. Rev. B* **1988**, *37*, 6482−6485.

DOI: 10.1021/jp510730a
J. Phys. Chem. C 2015, 119, 854−861